The Journal of Experimental Biology 208, 1435-1443
Published by The Company of Biologists 2005
doi:10.1242/jeb.01509

Propulsive force calculations in swimming frogs

I. A momentum–impulse approach

Sandra Nauwelaerts[1,*], Eize J. Stamhuis[2] and Peter Aerts[1]

[1]*Department of Biology, University of Antwerp, campus drie eiken, Universiteitsplein 1, B-2610 Wilrijk (Antwerpen), Belgium* and [2]*Department of Marine Biology, University of Groningen, Biologisch centrum, Haren, The Netherlands*

*Author for correspondence (e-mail: sandra.nauwelaerts@ua.ac.be)

Accepted 12 January 2005

Summary

Frogs are animals that are capable of locomotion in two physically different media, aquatic and terrestrial. A comparison of the kinematics of swimming frogs in a previous study revealed a difference in propulsive impulse between jumping and swimming. To explore this difference further, we determined the instantaneous forces during propulsion in swimming using an impulse–momentum approach based on DPIV flow data. The force profile obtained was compared with force profiles obtained from drag–thrust equilibrium of the centre of mass and with the force profiles generated during jumping. The new approach to quantifying the instantaneous forces during swimming was tested and proved to be a valid method for determining the external forces on the feet of swimming frogs.

On the kinematic profiles of swimming, leg extension precedes propulsion. This means that it is not only the acceleration of water backwards that provides thrust, but also that the deceleration of water flowing towards the frog as a result of recovery accelerates the centre of mass prior to leg extension.

The force profile obtained from the impulse–momentum approach exposed an overestimation of drag by 30% in the drag–thrust calculations. This means that the difference in impulse between jumping and swimming in frogs is even larger than previously stated. The difference between the force profiles, apart from a slightly higher peak force during jumping, lies mainly in a difference in shape. During swimming, maximal force is reached early in the extension phase, 20% into it, while during jumping, peak force is attained at 80% of the extension phase. This difference is caused by a difference in inter-limb coordination.

Key words: locomotion, swimming, frog, *Rana esculenta*, Anura, hind limb, DPIV, force.

Introduction

Much of what we know about animal locomotion is derived from studies that examined animals moving within single, homogeneous environments (Biewener and Gillis, 1999). However, many animals move through complex and heterogeneous physical environments at varying speeds and using different modes of locomotion. Obviously, animals must modulate their locomotor behaviour to adjust for changes in the external environment, resulting in changes in direction, speed or posture (Biewener and Corning, 2001; Irschick and Jayne, 1998). These resulting changes originate from the alteration of the force development during locomotion. The changes in force generation are expected to be most extreme for species that move through different physical environments, such as water *vs* land (Biewener and Gillis, 1999). In spite of these dramatic differences between aquatic and terrestrial environments with respect to several physical properties (Denny, 1993; Vogel, 1994), many animals succeed in using their limbs to locomote both in water and on land.

Green frogs *Rana esculenta* are semi-aquatic frogs that typically sit alongside small waterbodies, and will leap into the water when disturbed. Jumping and swimming seem equally important to this frog, making it an interesting model species with which to study the issue of how animals accommodate variability within the external environment.

In a previous study on the comparison of the kinematics of jumping and swimming of these semi-aquatic frogs, we were able to show that the propulsive impulse is much smaller during swimming (Nauwelaerts and Aerts, 2003). This difference in impulse was explained by four major hypotheses, which are not necessarily mutually exclusive. First, since we based our calculations of the propulsive impulse on the kinematics of the center of mass of the frog, we took into account only force components parallel to the direction of motion. It is possible that during swimming high *lateral* forces occur, causing the *resultant* force to be of similar magnitude for both swimming and jumping. A second explanation is an underestimation of the propulsive forces of swimming due to our calculation method. In our calculations, we estimated the

resistive force on an ellipsoid body that moved through the water according to the kinematics of a swimming frog. A reduced muscle recruitment, due to differences in the coordination patterns, was previously explored as a third option (Nauwelaerts and Aerts, 2003). Finally, a reduced force transmission due to a lower external load during swimming might explain the difference in propulsive impulse.

To test the first two hypotheses, quantification of the external forces on the feet during swimming becomes necessary. In a terrestrial environment, the ground reaction forces can be measured directly with a force platform, but measuring the forces exerted by organisms in an aquatic system is far more complex. To propel itself, a frog must interact with the surrounding water. The dynamic properties of the water and the swimming movements of the frog determine this interaction. The amount of thrust generated by the frog depends on the rate and the direction in which it changes the momentum of the surrounding water. One way of estimating the external forces is to study the flow induced by the frog's movements. This flow can be quantified using DPIV (Digital Particle Image Velocimetry). In this study, we will apply a momentum–impulse approach to estimate the propulsive forces on the feet during swimming. We will (1) evaluate this new approach for determining the instantaneous forces in water, (2) test the validity of the propulsive impulse quantifications in our previous study and (3) test whether higher lateral forces in swimming cause the difference in impulse between jumping and swimming.

Materials and methods

Animals

Five frogs *Rana esculenta* L. (snout–vent length 0.05±0.01 m, mass 0.015±0.03 kg) were caught in the wild at Groot Schietveld (Brecht, Belgium). The animals were housed in a glass terrarium and fed a diet of crickets. Temperature within the holding room was kept at 18°C, and a photoperiod of 12 h:12 h light:dark was maintained during the holding period. The Animal Care and Use Committee of the University of Antwerp approved both the animal housing and the experimental protocol.

Kinematics

In order to understand how the interaction between water and feet is realised, it is important to first map out the movements of the feet. The kinematical data were obtained similarly to the experiments described in Nauwelaerts and Aerts (2003). The sequences were recorded using a Redlake Motionscope system at 250 Hz. A mirror placed beneath the swimming tunnel allowed both ventral and lateral images to be recorded using a single camera. In this study we used the displacements of the digitisation points of ankle, mid-foot and toe tip. We also calculated the velocity and the acceleration of the centre of mass during the extension phase after using a digital filter with a cut-off frequency of 25 Hz. This phase was defined as the phase during which the foot moves backward in an earth-bound coordinate system and the leg joints are extended.

Minimal, maximal and the difference between minimal and maximal velocities were taken from the velocity profiles of swimming to test for differences in kinematics due to differences in velocity.

To obtain a full velocity range for each of the five animals, 32 sequences were selected for further analysis. For each sequence, ankle, mid-foot and toe tip were digitised, frame by frame, using an APAS (Ariel Performance Analyzing System). Stick figures of the movement of the foot in the vertical and horizontal plane were created from the digitisation data. A potential effect of velocity was tested using a correlation matrix. To test for individual differences, an ANOVA was performed. Both test were carried out in STATISTICA 5.1.

Experimental PIV setup

To record the propulsive flow generated by the hind limbs, each individual was placed in a glass container of 40 cm×30 cm×15 cm. This container was filled with water to a level of 14 cm. Neutrally buoyant Pliolyte particles with a diameter of approximately 25 μm (BASF, Leverkusen, Germany) were added to the water. The particles were illuminated by a laser light sheet using a red light Krypton laser (Coherent Innova K, Coherent Lasers Inc, Santa Clara, CA, USA; λ=647 nm; P_{max}=1 W) and a cylindrical lens (f=100 mm). To avoid video blurring from distortion of the water surface, a Perspex raft was placed on the water surface. The raft was shorter than the total length of the aquarium, allowing the animals to come to the surface and breathe at both sides, but forcing them to swim submerged in the middle of the tank.

Images of the illuminated particles were taken using a high speed video camera (Redlake MASD, Inc. San Diego, CA, USA) at 250 Hz, shuttered at 1/500 s. The sequences were recorded using two different sheet orientations: (1) a horizontal sheet 7.5 cm above the bottom of the tank, illuminating from behind and with the camera mounted above the aquarium, resulting in a dorsal view on the swimming frog, and (2) a vertical sheet with a lateral view on the frog, with a laser light illuminating from underneath the aquarium (using a mirror at an angle of 45°). In both cases the camera was mounted perpendicular to the laser sheet and in the middle of the tank.

Flow analysis

The flow patterns of swimming frogs were analysed on successive image pairs in Swift 4.0 (Dutch Vision Systems, Breda, The Netherlands) using an interrogation area of 51×51 pixels and 65% overlap between neighbouring areas. Convolution filtering was used as a method for image correlation analysis (Gonzalez and Wintz, 1987; Gonzalez and Woods, 1992). The displacement peak was located using a COGW method (centre of gravity weighted to grey value; Stamhuis et al., 2002). Calibration was performed using a plastic grid placed into the light sheet prior to the recordings. After manual data validation through the removal of erroneous

vectors and replacing these vectors using a 2D cubic natural spline interpolation (Spedding and Rignot, 1993; Stamhuis and Videler, 1995), the vector flow field containing information on the local velocity and direction of the flow was obtained. For each image pair, the velocity magnitude (expressed as a colour code between the minima and maxima) was superimposed on the vector diagram. Additionally, an isovelocity line of 0.05 m s^{-1} was calculated and drawn on the magnitude plots. This boundary at 5 cm s^{-1} was chosen after performing a sensitivity analysis on 20 magnitude plots.

Force calculations during swimming based on DPIV data

In each view, the isovelocity line on the magnitude plots comprised an area representing a slice through a volume of water with substantially elevated velocity. To investigate whether this area could be considered as an ellipse, we measured the area, the longest axis and width of this outlined area using Optimas 6.51 (Media Cybernetics, LP, Silver Spring, MD, USA). For each magnitude plot, we calculated the area of an ellipse defined by the length of these measured axes. We statistically verified whether there was a significant difference between the measured area and the calculated area of the ellipse using a paired data calculator (Westgard online tools).

To obtain the volume of the water mass affected by the frog's movements, the data from the two 2D views were combined. Since axis B (Fig. 1) was visible in both views, axes A and C could be defined in function of B. The volume of the affected water mass is then calculated as the volume of an ellipsoid body using two measured axes and one calculated axis. The mass of this volume M is simply the volume multiplied by the water density (1000 kg M^3) that is entrained by the foot and moves along with it.

The velocity of M was estimated by the velocity of the geometric centroid of the measured area, which equalled two thirds of the maximal velocity in the volume. This two thirds of the maximal velocity equals the average velocity when the velocity profile within the volume is elliptical. We decided to work with the velocity of the geometric centroid, because it was less subject to noise than the maximal velocity measured in the DPIV procedure. The impulse was calculated as the difference in momentum, $M\times$velocity, between two successive image pairs. Force is obtained by dividing this impulse by the time interval between two successive images (0.004 s). Since the two legs work independently, the total force is the calculated force multiplied by two (Stamhuis and Nauwelaerts, 2005).

The average force profile during swimming was obtained by first subdividing the total extension time into 21 equal steps by weighted interpolation, and then taking the average and standard deviation for each step from the eight sequences (Vereecke et al., 2003) from two animals.

Force profiles during swimming based on kinematical data

In order to compare the obtained force profile from the DPIV data with our previous calculations, we used seven kinematical sequences of one animal to calculate the propulsive forces. These calculations were based on the forces required to move an ellipsoid body with the dimensions of a frog's body through the water, while according it the movements of the centre of mass from the recorded swimming sequences (Nauwelaerts et al., 2001; Nauwelaerts and Aerts, 2003). The drag coefficient was determined from the deceleration during the glide phase. Because an overestimation of drag on an animal's body has previously led to false interpretations (Blake, 1983), we plotted the average force profile with and without drag.

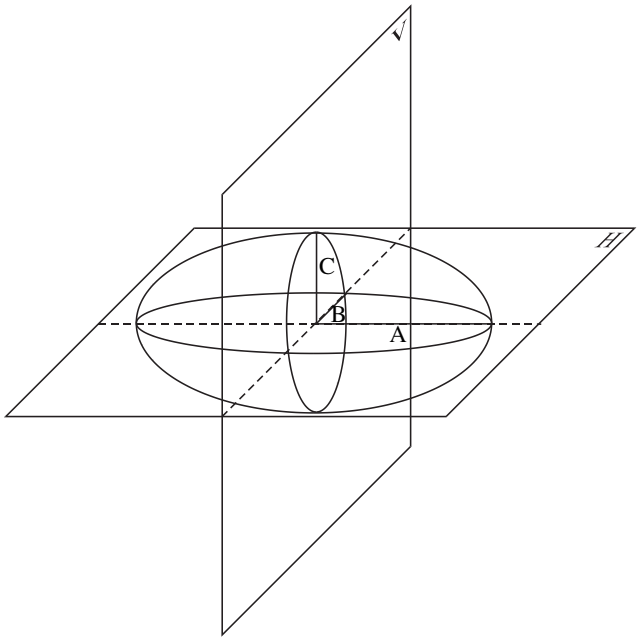

Fig. 1. An ellipsoid body, representing the water mass around the foot, is characterised by three axes, A, B and C. During the DPIV experiments, we used two sheet orientations (V, vertical; H, horizontal), which cut through the ellipsoid, creating a section with the shape of an ellipse characterised by two axes. Axis B belongs to both ellipses.

Force profiles during jumping

Frogs were placed upon a force plate (AMTI, MC3A-6-100, natural frequency 300 Hz). Slipping was prevented by covering the force platforms with water-resistant parquet sandpaper (P15U). To reduce noise, the force plate was placed in a plastic container filled with wetted sand. We sampled the ground reaction forces in three dimensions at 1000 Hz. To obtain a wide range of jumping distances, the jumping was either self-motivated or the frog was startled. The forces were reconstructed using the weighted interpolation method (see force calculations during swimming). Body weight was included in the propulsive force, since at any instant during the push-off phase, only forces above body weight can result in accelerations of the centre of mass. The average force profile of jumping was obtained similarly to the profile of swimming. The average of nine sequences of two frogs, together with its standard deviation (S.D.), was plotted against the relative time.

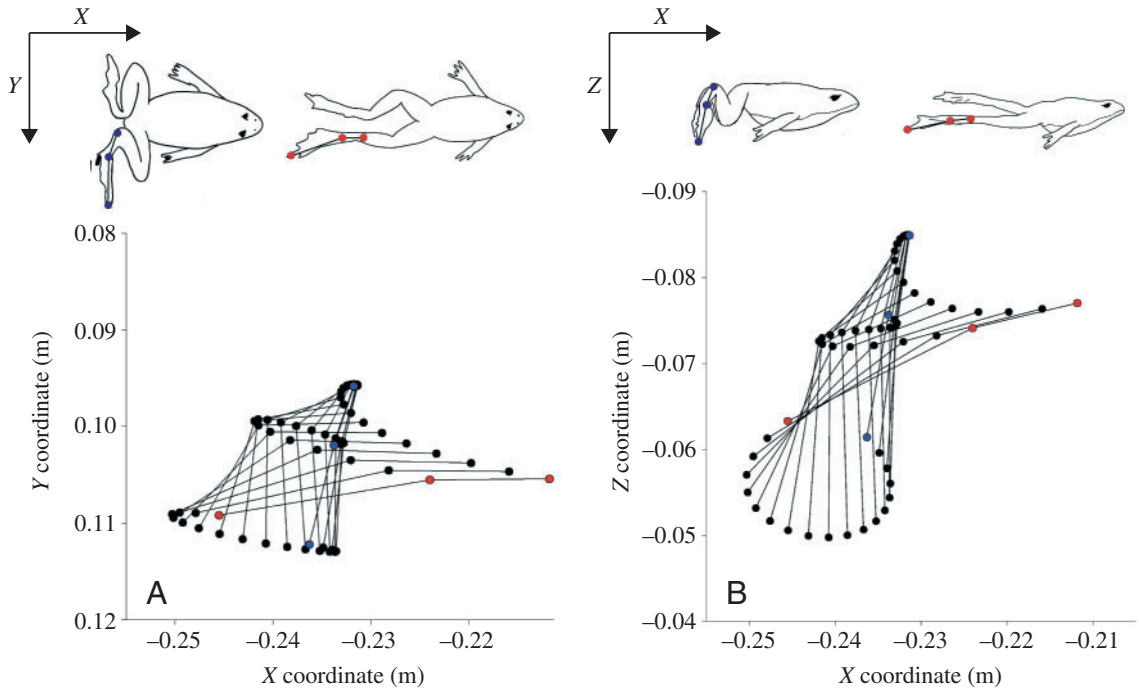

Fig. 2. Dorsal (A) and lateral (B) view on the stick figure (ankle–mid-foot–toe) of the leg of a swimming frog during leg extension. The blue circles show the joint positions at the start of the kick, the red ones represent the end of the kick. The time increment between two successive sticks is 0.004 s.

Results

Kinematics of the feet

Stick figures of the foot (Fig. 2) show a consistent pattern within both the horizontal and vertical planes. Since a similar pattern showed up for all animals (one individual was found to have smaller excursions of the toe tip, caused by the lack of the last toe segment – see Table 1) and at all speeds (if expressed as the difference between minimal and maximal velocity during propulsion), the results of only one sequence are presented graphically. The foot is placed perpendicular to the direction of movement. The direction of the line connecting ankle, mid-foot and toe tip is mostly oriented vertically, but is also slightly rotated outwards. The foot is pushed downwards and backwards, causing the webbing to flip over at the edges. After this, the foot (ankle and mid-foot) is extended, pulled up again and brought in line with the body. This means that although the ankle moves backwards very little (0.2 cm for the example shown) throughout the kick, the mid-foot (0.9 cm) and toe tip (1.7 cm) display substantial backwards movement.

Table 1. *Average displacements of ankle, mid foot and toe tip in the three dimensions of an earth-bound coordinate system*

	Displacement (m)								
Position	Frog 1	Frog 2	Frog 3	Frog 4	Frog 5	Mean	Maximum	Minimum	S.D.
Ankle									
X	4.864	7.542	4.937	1.593	3.762	4.201	18.820	0.0644	3.851
Y	3.818	4.908	4.436	2.387	6.584	4.418	13.760	0.704	3.304
Z	2.060	3.731	6.557	2.864	6.319	4.355	16.701	1.251	3.271
Mid-foot									
X	6.014	12.982	10.204	6.001	8.503	8.376	27.580	3.186	4.515
Y	3.343	3.526	4.305	1.872	4.603	3.469	11.814	0.754	2.223
Z	4.205	2.605	6.470	3.096	6.018	4.485	15.050	0.999	2.936
Toe									
X	12.215	17.35	21.966	19.940	25.041	19.678	31.217	4.605	6.797
Y	2.043	3.787	3.485	8.400	3.291	4.442	14.551	0.187	3.842
Z	10.754	8.332	8.142	12.460	10.676	10.374	19.446	1.778	4.427

X is the direction of movement, *Y* is lateral and *Z* is vertical displacement.

An effect of minimal speed on the kinematical patterns was found: the sideways mid-foot excursion was larger when the minimal speed was smaller (P=0.015, r=0.43).

Evaluation of the impulse–momentum approach

In both lateral and dorsal views (Fig. 3), a mass of water is created around the foot at the start of the extension phase and as the backward velocity increases, the volume increases. Since we measured both the cross-sectional area of the moving water volume and the axes of the ellipse directly, we could test the accuracy of the ellipsoid approach by comparing the measured and the calculated areas ($\pi\times0.5$axis1$\times0.5$axis2) in both views. The observed bias is small (–0.64 cm^2 for the horizontal sequences and –0.35 cm^2 for the vertical ones) but significant (t=–6.6210, N=40, P<0.01 and t=–3.7699, N=27, P>0.01, respectively), showing that the ellipse approach overestimates the area slightly and systematically by 10±2% in the horizontal plane and 8±2% in the vertical plane, which makes this approach overestimate the volume by 19±3%. On the other hand, a slight underestimation is possible in the measured areas because the boundaries of the affected volume were measured at 0.05 m s^{-1} for practical reasons (theoretically the boundaries would have been at 0 m s^{-1}). Since both effects are small and have an opposite sign, they are assumed to neutralise each other.

The length of the three axes of the ellipsoid is time dependent, but no overall relation with speed was found. Axis A, the major axis in the dorsal view (average length 0.033±0.013 m), has a parabolic time dependency, with an increase in size to a maximum halfway through the extension phase. The maximum length of A equals the total length of the foot. Axes B and C are of similar size (average lengths 0.025±0.013 m and 0.023±0.008 m, respectively).

At the start of the extension phase, the velocity of the mass (average velocity at the start of propulsion phase

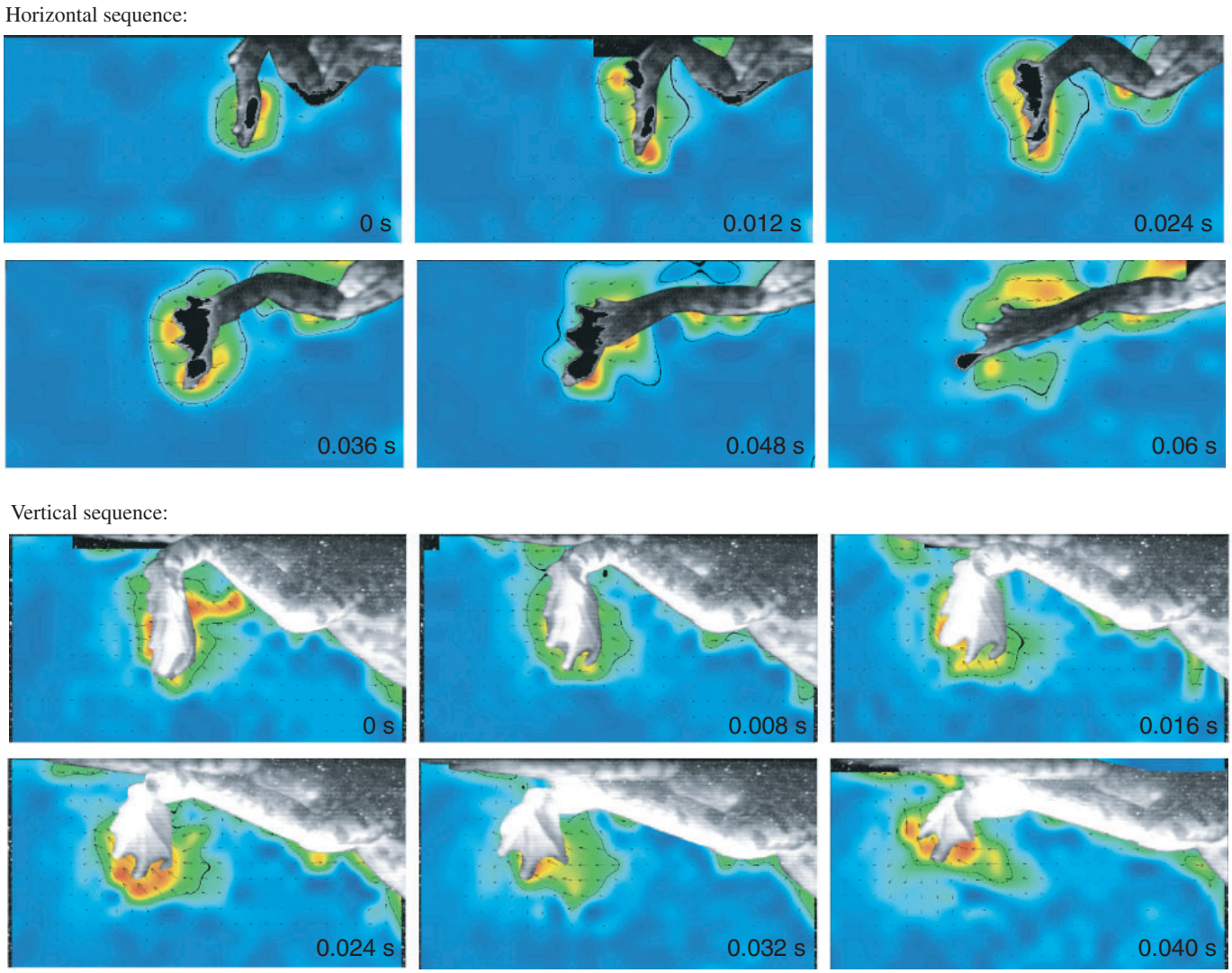

Fig. 3. Vector diagram of the flow around a swimming frog in two perpendicular views. Each vector shows the direction and relative magnitude of the velocity of the local flow. Maximal velocity is colour coded red, minimal velocity (around zero) is shown in blue. The top sequence results from a DPIV analysis of a sequence with a horizontal laser sheet orientation, the bottom sequence with a vertical laser sheet orientation. From each sequence, six images distributed equally over the whole kick are shown.

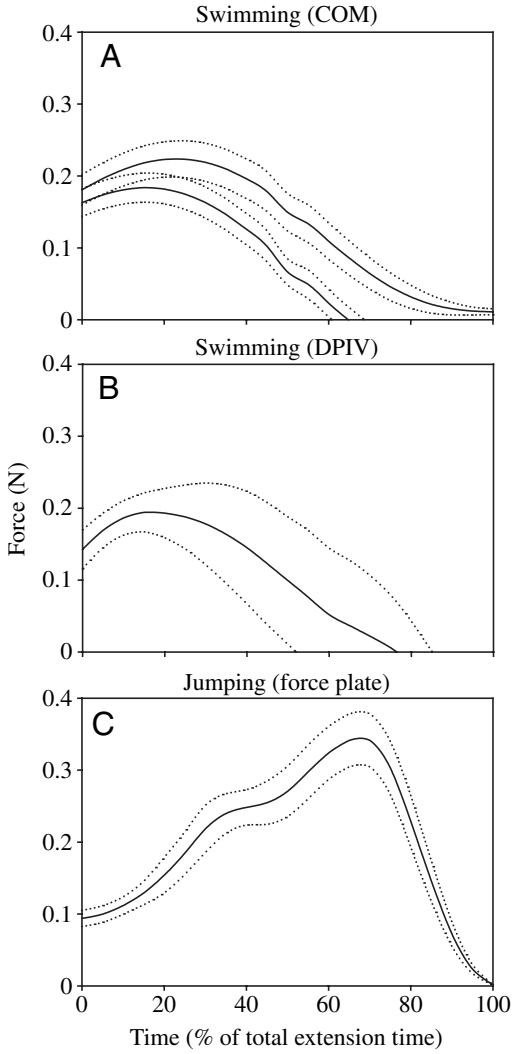

Fig. 4. Force profile in N on the feet of a swimming frog through time in % of total extension time. Average force profile is shown as a solid line; dotted lines indicate ± S.D. (A) Calculated based on the displacements of the centre of mass (COM) of the frog with and without drag. (B) Measured using an impulse–momentum approach based on the DPIV data. (C) Measured using a force plate.

is 0.122±0.05 m s^{-1}) equals the velocity of the foot (0.124±0.08 m s^{-1}), but as the foot is pulled out of the mass in the course of extension and moved upwards and forward, the mass continues to move in the same direction, decelerating slightly (at 3±1 m s^{-2}) due to its interaction with the foot and the surrounding water.

Lateral forces

The lateral forces can be estimated in the same way as the propulsive forces, but using the displacement of the centroid perpendicular to the direction of motion. The displacement of the centroid of the measured area occurred almost entirely in the direction of movement of the body, the *X* direction: the total displacement in the *Y* (horizontal) and *Z* directions (vertical) was on average 21±5% of the displacement in the *X* direction,

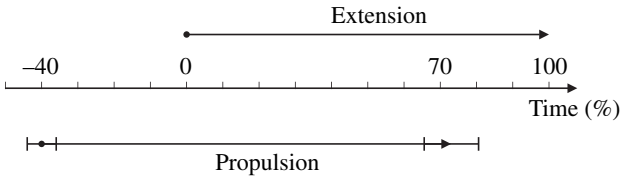

Fig. 5. Schematic diagram of the time lag between propulsion and extension. Extension duration is expressed in percentages, from 0 to 100. Propulsion is expressed as a fraction of total extension time and starts at 42±8% (mean ± S.D.) before extension and ends at 71±15% of extension.

which means that in both in the dorsal and lateral views, the resultant thrust force makes an angle of 11±3° with the direction of movement.

Force profile during swimming

The average force profile for swimming (Fig. 4A,B) shows that a considerable forward-directed force acting on the frog already exists before the start of the extension phase and lasts during the first 75% of the extension phase. In the last quarter of the extension phase, the estimated force becomes negative, indicating that the mass of water no longer interacts with the almost fully extended foot, but that during this last part, the foot is pulled out of this volume of water, leaving behind a vortex ring (see Stamhuis and Nauwelaerts, 2005).

Centre of mass calculations

The force profile based on the DPIV measurements was compared with the propulsive force calculations based on the acceleration of the centre of mass (COM) that were used in previous studies (Nauwelaerts et al., 2001; Nauwelaerts and Aerts, 2003). In Fig. 4A is plotted the average force profile based on the acceleration of mass, with and without drag. The force profile obtained from the DPIV measurements falls between the two force profiles of the COM (Fig. 4B). Consequently, it is possible that drag was overestimated in our previous calculations. This means that the real difference in impulse between swimming and jumping may be even larger than previously stated.

As shown in Fig. 4A,B, the propulsive force during swimming does not start at zero at the start of the extension phase. The timings of (1) the acceleration of the centre of mass with (2) the extension phase, do not overlap (see Fig. 5). If the extension phase is defined as the phase during which the hind limbs move backwards, and the propulsion phase as the phase in which the centre of mass accelerates, then propulsion precedes leg extension and ends before extension is completed. The propulsion phase starts on average at –42% of the extension phase (±8% S.D.) and ends at 71% (±15%), based upon 33 kinematic sequences (Fig. 5).

Swimming and jumping

The force profile of swimming was compared with the average force profile obtained from the ground reaction force measurements using the force plate (Fig. 4C). The average

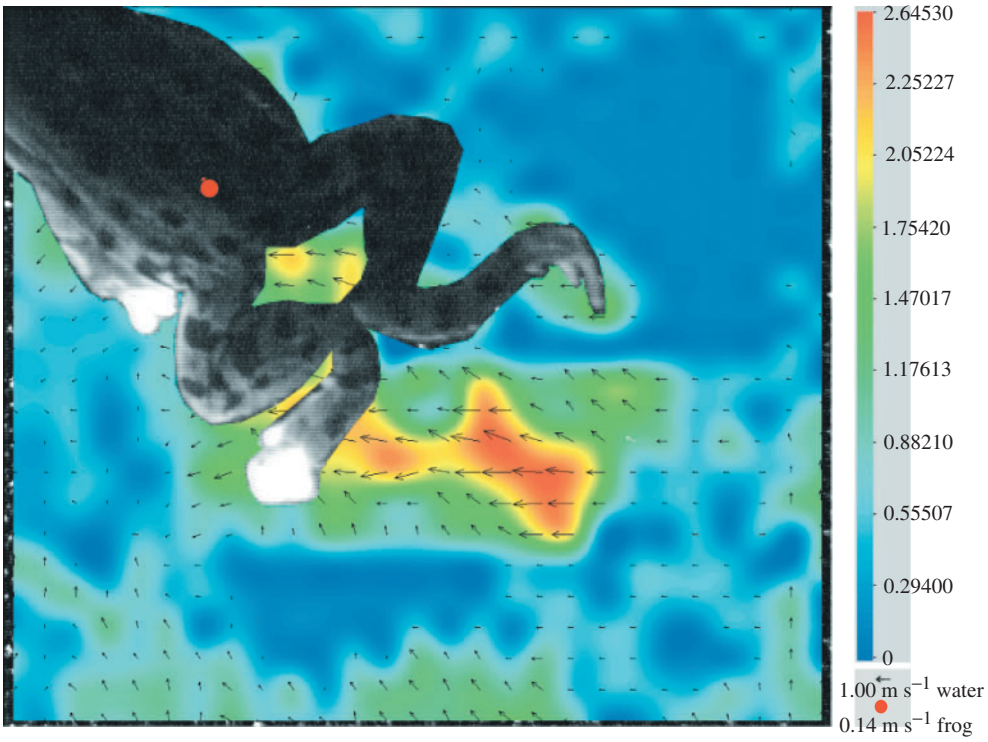

Fig. 6. Vector diagram of the flow around a swimming *Rana esculenta* results from a digital particle image velocimetry (DPIV) analysis. Each vector shows the direction and relative magnitude of the velocity of the local flow. Maximal velocity is colour coded red, minimal velocity is shown in blue. Extension is not yet initiated and thrust is obtained by slowing down the flow coming towards the frog. This flow is generated during recovery, i.e. flexing the hind limbs behind the frog's body.

maximal force for jumping is 0.38±0.09 N (variance=0.008) and is significantly larger than that measured for swimming (0.26±0.12 N, variance=0.015) when tested with a *t*-test assuming unequal variances (one-tail test, P=0.028; two-tail test, P =0.055). During swimming, this maximal force is reached early in the extension phase, at 20±6% of the total extension time, while the timing of the maximal force is during jumping is postponed until late in the extension phase, at 70±12% of the total extension time.

Discussion

In our impulse–momentum approach, we consider the fluid dynamic force to consist primarily of the fluid momentum. The frog accelerates a volume of water backwards by applying force to the surrounding water. At the same time, a shear layer is created between the stationary water and the moving fluid due to viscous friction between the moving volume and the surrounding water. We, however, decided to ignore the contributions from shear, because the vorticity was found to be negligible during the kick phase: the vorticity intensity near the foot never exceeded the background noise levels. In case of the frog, moving its feet with a Reynold's number Re of about 15 000 (or even higher), we feel that we can relatively safely assume that the viscous forces are confined to a thin boundary layer only. Hardly any vorticity is shed during the kick, and the vorticity that is bound to the foot ends up in a free vortex ring that is shed as soon as the frog's foot stops to accelerate. The impulse of these vortex rings can be used to calculate the average propulsive force (Stamhuis and Nauwelaerts, 2005). A paired comparison of the resulting average thrust was possible for two sequences (Frog 1: 0.148 N *vs* 0.130 N, vortex ring approach *vs* impulse approach; Frog 2: 0.069 N *vs* 0.082 N), which shows good agreement between the two methods, adding credibility to the calculation method presented here. In previous studies, an inviscid approach resulted in an underestimation of the calculated thrust forces compared to measured forces for a robotic insect moving at Re≈150 (e.g. Sane and Dickinson, 2001). We find a better match between different methods, probably due to two effects: a different Reynolds number and a different kinematical pattern of the propulsive apparatus. Frogs feet move at a Reynolds number of 15 000, clearly in the inertial regime, and they move mainly by translating perpendicular to the flow.

Frogs swim by accelerating a mass of water backwards. The size of this mass of water is time dependent, but we found no dependency on the velocity of the frog's foot. This is probably due to the fact that such dependency exists only in the first half of the extension phase, when the mass of the affected water is increased. Once the maximal volume is established, the foot is pulled out of the mass and therefore the dependency on the foot velocity is removed. The propulsive forces are only delivered by the kicking legs during the first 70% of the extension phase. Surprisingly, however, thrust is already present before the start of the extension phase. During the recovery phase, the phase during which the legs are retracted behind the body, some adherent water is dragged along in the direction of motion. This water mass is being slowed down abruptly by the feet when their webbings are spread and placed perpendicular in this flow. The mass's velocity is reversed when the feet start moving backwards. This mechanism of decelerating a forward moving mass of water provides extra propulsion before the legs

start to extend. Quantification of this additional thrust is not possible at this stage. A similar impulse–momentum approach is certainly possible, but requires a different recording strategy; with attention being focused on the recovery phase. In addition, the mass that is dragged forward lies between the legs. To quantify this water mass, it is therefore important to have both the legs in view. Even without quantifying this additional thrust, we still have strong indications that the mechanism described above is realistic. Fig. 6 shows that a water mass moves towards the frog during leg flexion. This water mass disappears during the next phase when the frog spreads its webbings perpendicular to this incoming flow, in this way generating thrust even before the extension phase begins. We cannot exclude the possibility that the slowing down of the flexing legs also adds to this extra thrust before extension. However, deceleration of the legs probably coincides with relaxation of the leg muscles, and it is therefore more probable that the deceleration would result in a further, passive, flexion of the legs.

Estimating the propulsive forces generated by the locomotor apparatus of a swimming frog from the observed acceleration profile of the centre of mass and the drag on the frog's body seems to imply a few pitfalls. Both in our calculations (Fig. 4A, profile with drag) and in the calculations of Gal and Blake (1988a,b), both based on the acceleration of the centre of mass, the estimate of the total propulsive force remained positive throughout hind limb extension. Although the force calculations show thrust for the entire extension phase, the acceleration of the frog's centre of mass becomes negative after 70% of the total extension time (Fig. 4B, profile without drag). This discrepancy originates from summing the force due to the acceleration and the drag force. An overestimation of this drag force, as shown here (Figs 4A and 5), causes the total thrust to remain positive and shifts its timing to later in the extension phase, ultimately to the end of the extension. We used a drag coefficient calculated from the deceleration of the centre of mass during the glide phase, while Gal and Blake (1988a) used data from drop-tank tests. The inaccuracy of the acceleration profile of the centre of mass may also add to this prolonging of the positive thrust. Taking derivatives of the measured coordinates twice necessitates the use of a filter algorithm and can result in a broadening of the acceleration peak. The overestimation of the propulsive forces during swimming in our centre of mass calculations implies that, in reality, the impulse during swimming will be even smaller. The difference in impulse between jumping and swimming is therefore even larger than first stated (Nauwelaerts and Aerts, 2003).

Using a blade-element approach, Gal and Blake (1988b) calculated the propulsive forces in the direction of motion, based on the hind limb kinematics of a swimming *Hymenochirus boettgeri*, an aquatic frog. The hind limb was modelled as a series of linked three-dimensional circular cylinders and a flat plane, in free flow. The assumption of the circular cylinders causes a slight deviation from the observed ellipsoid mass of water moved by the feet in our DPIV measurements, but the model generally holds true. The force profile they obtained using this model strongly resembles our own: propulsion starts before extension and decreases about halfway the extension phase. The maximal force peak measured by Gal and Blake (1988b) is much smaller than ours (0.001 N *vs* 0.26 N, respectively). Unfortunately, the study does not mention the size of the frogs, but *H. boettgeri* is known to be a small species compared to *Rana esculenta*. Gal and Blake (1988b) also compared the thrust profile from their model with the force profile obtained from the force balance between thrust and drag, and concluded that a simple drag-based propulsion system may not be sufficient to describe the locomotor behaviour of frogs. Gal and Blake (1988b) suggested that two mechanisms are at work during leg extension: a reflective and a jet effect. Both effects result from the interaction between the two limbs. We were able to show that these mechanisms are absent (E. Stamhuis and S. Nauwelaerts, manuscript submitted for publication). Johansson and Norberg (2003) suggested a lift-based swimming technique for frogs. However, the lack of downwash, the small lateral forces and the angle of attack of the foot that was perpendicular to the direction of movement convinced us that frogs use a drag-based propulsion system during swimming. We believe that it was not Gal and Blake's model – based on the kinematics of the hind limbs – that failed, but that the estimation of the propulsive forces from the force balance lacked accuracy, both in their calculations and in our own (Nauwelaerts and Aerts, 2003).

The impulses for jumping are about twice the size of those for swimming (Nauwelaerts et al., 2003). The difference is caused by an increase in maximal force (0.38±0.09 N for jumping *vs* 0.26±0.12 N for swimming) and by the difference in shape of the force-time curve. During swimming, the maximal force is reached early in the extension phase (Fig. 4A,B), while the timing of the force peak during jumping is postponed until the end of the extension phase (Fig. 4C). The impulse equals the change in momentum, which is the product of velocity and mass. In order to increase the impulses during swimming and shift them into the impulse range of jumping, there are only two options. The first option is an increase in the *velocity* of the mass, which implies an increase in contraction rate of the muscles. Due to the smaller external load during swimming, a higher extension velocity is expected, but was not found (Nauwelaerts and Aerts, 2003). It is possible that the maximal extension velocity the muscles can realise during swimming is lower than expected in comparison with jumping, due to the difference in coordination (Nauwelaerts and Aerts, 2003). During jumping, a proximo-distal sequence in joint extension occurs: the hip precedes the extension of knee and ankle. This joint succession ensures a prolonged acceleration of the centre of mass. The ground reaction peak force is reached late in the extension phase (Fig. 4C), close to take-off, and take-off occurs when the body is fully extended. If all joints had extended simultaneously, as occurs during swimming, higher extension velocities would have been reached (Alexander, 1989), but due to geometrical constraints

of the extending joints, the timing of the maximal force would have been unfavourable (van Ingen Schenau, 1989). During swimming, the timing of the maximal force seems to be of less importance, because no specific benefit is gained from achieving maximal velocity at any particular moment the extension phase. In addition, because of the horizontal position of the frog's trunk, an early extension of the hip, without an extension of the other joints would result in a kick upwards. The outcome would be either a tilt of the trunk, or a smaller propulsion force, due to a higher lateral force. The second option that could increase the impulse during swimming is an increase in *mass*. The maximal size of the ellipsoid mass is limited by the morphology of the foot. Spreading the web and extending the toes can actively increase the size of the mass surrounding the feet. In order to maintain the maximal size of this water volume, the feet have to be kept in the same posture, even when high forces are acting on them. This means that during swimming it is important to keep the feet as rigid as possible and perpendicular to the flow. This is in contrast with the necessary flexibility of the feet during the roll-off at the end of the extension phase during jumping.

Since the impulses of swimming and jumping also differ when the calculations for swimming are based upon DPIV measurements, we have to reject the possibility that our calculation method (Nauwelaerts and Aerts, 2003) caused the difference. This leaves us with the possibility that the lateral forces are larger during swimming, causing the resultant force to be of similar magnitude to the resultant force of jumping. On the basis of our current findings, we also have to reject this hypothesis. In both planes, there is almost no displacement of the mass in the direction perpendicular to the direction of motion. This indicates small lateral forces.

We have collected the propulsive force profiles in each method slightly differently, which could potentially cause a difference in profile shape. The swimming force profile based on the kinematics was from one animal, using seven sequences over a wide velocity range. The one based on DPIV data came from two animals, using eight sequences at intermediate velocity. Finally, the force profile for jumping consisted of data from nine sequences of two animals over a wide range of distances. This difference in approach was for practical reasons. The data obtained over a wide range of performances should inevitably yield more variation. But, we do not believe that this difference in motivation could be the only cause of the large difference in force profile between jumping and swimming.

In conclusion, frogs use a drag-based propulsion system during swimming. We slightly overestimated drag in our previous impulse calculations (Nauwelaerts and Aerts, 2003), suggesting the difference in impulse between jumping and swimming to be even larger than first stated. This impulse difference is mainly caused by a difference in shape of the thrust–time curve, which in turn can be explained by a difference in inter-limb coordination. The coordination of jumping follows the optimisation theories of maximal jumping, but this coordination cannot be used during swimming, because an early hip extension would cause the frog to pitch upwards.

This study was supported by a grant of IWT-Vlaanderen and an ISB Travel grant.

References

Alexander, R. McN. (1989). Sequential joint extension in jumping (Reaction to G. J. van Ingen Schenau, 1989). *Hum. Movement Sci.* **8**, 339-345.

Biewener, A. A. and Corning, W. R. (2001). Dynamics of mallard (*Anas platyrhinchos*) gastrocnemius function during swimming *versus* terrestrial locomotion. *J. Exp. Biol.* **204**, 1745-1756.

Biewener, A. A. and Gillis, G. B. (1999). Dynamics of muscle function during locomotion: accommodating variable conditions. *J. Exp. Biol.* **202**, 3387-3396.

Blake, R. W. (1983). *Fish Locomotion*. Cambridge: Cambridge University Press. 208pp.

Denny, M. W. (1993). *Air and Water.* Princeton: Princeton University Press.

Gal, J. M. and Blake, R. W. (1988a). Hydrodynamic drag of two frog species: *Hymenochirus boettgeri* and *Rana pipiens*. *Can. J. Zool.* **65**, 1085-1090.

Gal, J. M. and Blake, R. W. (1988b). Biomechanics of frog swimming. II. Mechanics of the limb-beat cycle in *Hymenochirus boettgeri. J. Exp. Biol*. **138**, 413-429.

Gonzalez, R. C. and Wintz, P. (1987). *Digital Image Processing*. Reading, MA: Addison-Wesley.

Gonzalez, R. C. and Woods, R. E. (1992). *Digital Image Processing*. Reading: Addison-Wesley Publishing Company.

Irschick, D. J. and Jayne, B. C. (1998). Effects of incline on speed, acceleration, body posture and hindlimb kinematics in two species of lizard *Callisaurus draconoides* and *Uma scoparia*. *J. Exp. Biol.* **201**, 273-287.

Johansson, L. C. and Norberg, R. A. (2003). Delta-wing function of webbed feet gives hydrodynamic lift for swimming propulsion in birds. *Nature* **424**, 65-68.

Nauwelaerts, S. and Aerts, P. (2003). Propulsive impulse as a covarying performance measure in the comparison of the kinematics of jumping and swimming in frogs. *J. Exp. Biol.* **206**, 4341-4251.

Nauwelaerts, S., Aerts, P. and D'Aout, K. (2001). Speed modulation in swimming frogs. *J. Motor Behav.* **33**, 265-272.

Sane, S. P. and Dickinson, M. H. (2001). The control of flight force by a flapping wing: lift and drag production. *J. Exp. Biol.* **204**, 2607-2626.

Spedding, G. R. and Rignot, E. J. M. (1993). Performance analysis and application of grid interpolation techniques for fluid-flows. *Exp. Fluids* **15**, 417-430.

Stamhuis, E. J. and Nauwelaerts, S. (2005). Propulsive force calculations in swimming frogs. II. A vortex ring approach. *J. Exp. Biol.* **208**, 1445-1451

Stamhuis, E. J. and Videler, J. J. (1995). Quantitative flow analysis around aquatic animals using laser sheet particle image velocimetry. *J. Exp. Biol.* **198**, 283-294.

Stamhuis, E. J., Videler, J. J., van Duren, L. A. and Muller, U. K. (2002). Applying digital particle image velocimetry to animal-generated flows: traps, hurdles and cures in mapping steady and unsteady flows in Re regimes between 10(–2) and 10 (5). *Exp. Fluids.* **33**, 801-813.

van Ingen Schenau, G. J. (1989). From rotation to translation: Constraints on multi-joint movements and the unique action of bi-articular muscles. *Hum. Movement Sci.* **8**, 301-337.

Vereecke, E., D'Août, K., DeClercq, D., Van Elsacker, L. and Aerts, P. (2003). Dynamic plantar pressure distribution during terrestrial locomotion of Bonobos (*Pan paniscus*). *Am. J. Phys. Anthropol.* **120**, 373-383.

Vogel, S. (1994). *Life in Moving Fluids.* Princeton: Princeton University Press.